

Observation of Inter-layer Excitons in MoSe₂ Single Crystals

Jason Horng, Long Zhang, Eunice Y. Paik, and Hui Deng
Physics Department, University of Michigan, 450 Church Street, Ann Arbor, MI 48109-2122, USA

Tineke Stroucken and Stephan W. Koch
Department of Physics and Material Sciences Center, Philipps University Marburg, Renthof 5, D-35032 Marburg, Germany
(Dated: January 22, 2022)

Interlayer excitons are observed coexisting with intralayer excitons in bi-layer, few-layer, and bulk MoSe₂ single crystals by confocal reflection contrast spectroscopy. Quantitative analysis using the Dirac-Bloch-Equations provides unambiguous state assignment of all the measured resonances. The interlayer excitons in bilayer MoSe₂ have a large binding energy of 153 meV, narrow linewidth of 20 meV, and their spectral weight is comparable to the commonly studied higher-order intralayer excitons. At the same time, the interlayer excitons are characterized by distinct transition energies and permanent dipole moments providing a promising high temperature and optically accessible platform for dipolar exciton physics.

The basic understanding of spatially direct semiconductor excitons dates back to the 1930s [1, 2], where an exciton in a single crystal has been described as a Coulomb bound pair of an electron and a hole that spatially overlap in the absence of external electrical or magnetic fields. To create spatially indirect excitons, heterostructures were used, first with coupled GaAs quantum wells [3, 4] and more recently with stacked van der Waals crystal systems (vdWcs) [5–11].

Here, we use confocal reflection contrast spectroscopy to show that stable, indirect exciton resonances exist in multilayer single crystals of MoSe₂. In these interlayer excitons, the electron and hole are confined to neighboring molecular layers and the associated optical resonances are shown to coexist with those of the usual intralayer excitons. Mono-, bi-, tri- and few-layer up to bulk crystals on the same substrate are studied systematically and bilayer results are presented with and without encapsulation.

The experimental spectra are analyzed by numerically solving the coupled microscopic gap and Dirac-Bloch equations [12, 13]. For all structures, the agreement between the theory and experiment is fully quantitative and allows for an unambiguous state assignment.

The identification of interlayer excitons enriches our basic understanding of the optical and electrical properties of van der Waals crystals. Furthermore, these interlayer excitons promise a new platform for non-equilibrium many-body physics. Similar to indirect excitons in heterostructures, they have a permanent, aligned dipole moment that leads to long-range dipole-dipole interactions and a wide range of associated quantum many-body phenomena [14–19].

Due to their permanent dipole moment, indirect excitons in conventional semiconductor heterostructures are sensitive to local electronic disorders including those at the internal interfaces of the heterostructures. They also have a greatly reduced binding energy and optical transition rate, limiting their operation temperatures and experimental accessibility. In contrast, interlayer excitons in monocrystalline vdWcs do not experience internal interfaces. Furthermore, the external crystal surfaces can be very effectively passivated by hexagonal-boron-nitride (hBN) layers. These near ideal structural con-

ditions reflect themselves in the measured narrow linewidth of 19 meV, which is comparable to that of intra-layer excitons and many times narrower than indirect excitons in vdWc heterostructures. Moreover, due to the close proximity of the neighboring molecular layers, the interlayer excitons maintain a relatively large exciton binding energy, 153 meV in MoSe₂. Therefore, they may allow dipolar exciton studies at the presence of relatively high doping densities and temperatures. The interlayer excitons also remain optically active, which will enable convenient optical access to the system and potentially powerful cavity effects [20, 21]. While it will also result in a relatively fast radiative decay and restricts the system to non-equilibrium regime, quantum many-body phenomena have been shown to survive in non-equilibrium systems. Lastly, bi-layer and few-layer vdWcs are easier to fabricate than heterostructures and do not suffer from lattice mismatch or angle rotation between the constituting lattices.

In Fig. 1(a), we schematically show the real-space config-

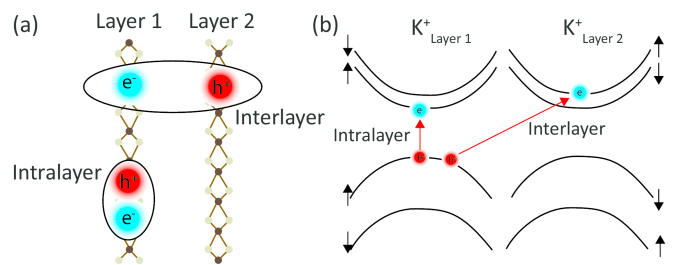


FIG. 1: Schematic illustration of inter- and intralayer excitons in transition-metal-dichalcogenides (TMD) multilayers. (a) real-space representation of different species of excitons. Interlayer excitons consist of an electron and a hole in different layers, while the intralayer exciton consists of an electron and a hole in the same layer. (b) k-space and spin configuration for optically bright interlayer and intralayer excitons. The arrows indicate the dipole allowed transitions at the K-point of the joint Brillouin zone corresponding to the A-exciton series. At the K^+ points, the layer indices are reversed.

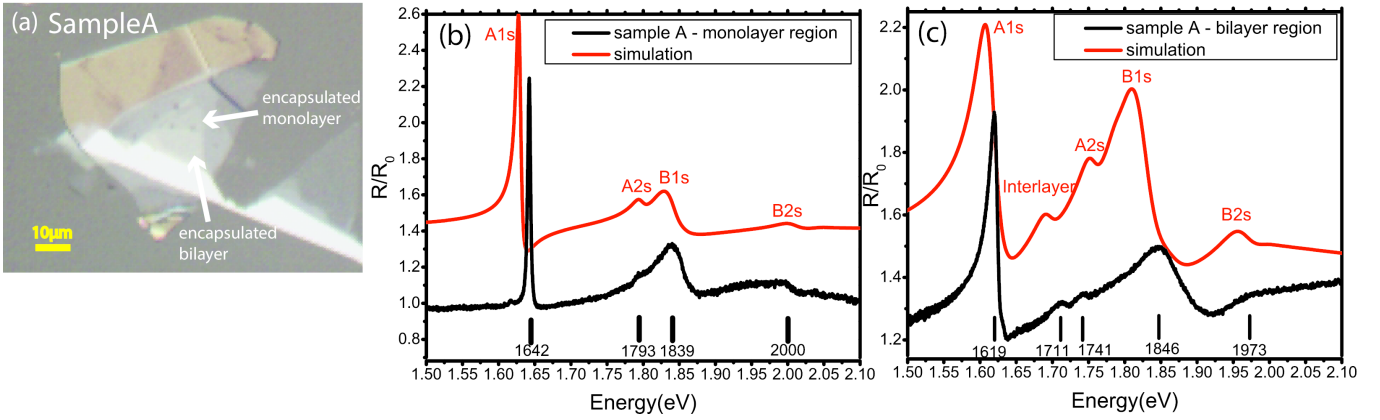


FIG. 2: (a) Optical microscope image of sample A, consisting of hexagonal boron nitride (hBN) encapsulated MoSe₂ layers. The red and black dash line indicate the encapsulated monolayer and bilayer region. (b) and (c) Measured (black curve) and simulated (red curve) reflection contrast spectra ($R/R_0(E)$) from encapsulated monolayer (in (b)) and bilayer (in (c)) region of sample A, where $R(E)$ and $R_0(E)$ are reflection spectrum from sample and substrate area. The experimentally observed peaks are labeled with their resonance energies. Simulated optical spectra are based on DBE and a four-band effective Hamiltonian. Comparing experiment and theory, we assign the peaks from low to high energy as A_{1s} , A_{2s} , B_{1s} , B_{2s} for the intra-layer excitons and identify the new peak at 1711 meV in the bilayer as the inter-layer A_{1s}^{inter} exciton. All simulated spectra have been shifted for better visibility.

uration of the interlayer exciton in a MoSe₂ bilayer. Even though the transition from a direct to indirect gap in most vdWc multilayer structures already occurs for the bilayer, the direct gap at the K -points of the Brillouin zone is preserved even in the bulk limit, with a dispersion that is flat along the $K-H$ direction[22]. This flat dispersion indicates that even in a multilayer structure, the near K -point quasi-particles can be considered as effectively two-dimensional, and are strongly confined within individual layers, with the potential to build bound interlayer excitons even in multilayer structures consisting of identical monolayers.

In Fig. 1(b), we show the band and spin configuration for the non-interacting band structure around the K^+ -point in an A-B stacked MoSe₂ bilayer. Whereas the K^\pm -points of a monolayer are nonequivalent and related by the parity transformation, they are equivalent in an inversion symmetric bilayer. At each K -point, the non-interacting bandstructure is composed of the spin-split valence and conduction bands of layer 1 and a mirror identical copy with reversed spin ordering of layer 2[23]. Consequently, dipole allowed intralayer excitons corresponding to the A-series in MoSe₂ are formed by an electron in the lowest conduction band and a hole in the highest valence band, whereas the correspondent interlayer exciton uses the upper spin-split conduction band (see arrows in Fig. 1(b)). Thus, the optical selection rules for the interlayer excitons exhibit similar symmetry properties as those for the intra-layer excitons with the difference that the spin-valley selectivity in a monolayer is replaced by spin-layer selectivity for the excitation with circular polarized light.

To experimentally identify interlayer excitons in vdWc multilayers, we perform confocal reflection spectroscopy with a tungsten lamp source at 5 K to study the bound

electron-hole pairs on MoSe₂ flakes with a spatial resolution of 2 μm . Signals from the sample were normalized against a point on nearby substrate to produce reflection contrast. Fig. 2(a) shows an optical microscope image of sample A, consisting of an hBN-encapsulated monolayer and bilayer MoSe₂. The measured reflection contrast spectrum (R/R_0) for the monolayer region on this sample is shown as black curve in Fig. 2(b), where R and R_0 are reflection spectrum taken from sample and substrate area, respectively. A typical spectrum of monolayer MoSe₂ was observed with reflection peaks corresponding to A_{1s} (1642 meV) and B_{1s} (1839 meV) excitons. Due to the sharp linewidth resulting from the hBN encapsulation, we can also identify the excited excitons A_{2s} at 1793 meV and B_{2s} at 2000 meV, both with much smaller oscillator strengths relative to the $1s$ states. Because of the rapid decrease of spectral weight with increasing quantum number and interference between different species of excitons, we cannot resolve the $3s$, $4s$, ... excitons states experimentally.

The corresponding optical spectrum in the encapsulated bilayer region is shown in Fig. 2(c). The bilayer spectrum has somewhat broader A_{1s} and B_{1s} resonances and we note a red shift of the dominant A_{1s} resonance of 23 meV and a small blue shift of the B_{1s} resonance of 7 meV, respectively. Strikingly, we also observe two additional peaks above the A_{1s} transition at 1711 meV and 1741 meV with similar oscillator strength, and a weak spectral feature at 1973 meV. Naively, one could try to assign the two peaks above the A_{1s} resonance to the A_{2s} and A_{3s} exciton resonances that are red shifted by the presence of the second layer. However, this assignment is unreasonable due to the similar oscillator strength of the two observed peaks.

To understand the physical origin of the observed features,

we employ the theoretical framework that combines an electrostatic model for the Coulomb interaction potential in an anisotropic medium, i.e. the gap equations to determine the interacting gap, and the Dirac-Bloch-Equations (DBE) to compute the linear optical response[12]. Within this model, the electronic and optical properties around the K-points of the multilayer structures are treated by considering the symmetry induced spin locking of the individual layers and the inter- and intralayer Coulomb interaction. Treating the Hamiltonian of the isolated monolayer within an effective four-band model[24], screening of the bands under consideration is included dynamically, whereas screening of all remaining bands and the dielectric environment is contained in the Coulomb matrix element. The material parameters used are listed in Ref. [25]. This model is based on the observation that the direct gap at the K-points, which contributes dominantly to the optical absorption, is preserved while increasing the number of layers from a monolayer to bulk [22]. At the K points, the out-of-plane effective masses of the valence and conduction bands are typically much larger than those in the in-plane directions. Consequently, the out-of-plane component of the kinetic energy can be neglected and the quasi-particles at the K-points can be considered as quasi-two dimensional, well confined within the layers. These assumptions are strongly supported by recent ARPES measurements, which have revealed the two-dimensional nature of the bands at the K point of the Brillouin zone [26]

The theory predicts the resonance positions $A_{1s} = 1642$ meV and $A_{2s} = 1802$ meV at zero density and temperature respectively, which shift to $A_{1s} = 1629$ meV and $A_{2s} = 1796$ meV in the presence of a small carrier density of $n = 1.3 \cdot 10^9/\text{cm}^2$. The computed optical spectrum for the encapsulated monolayer is plotted in Fig. 2(b) for comparison with the experiment. In the numerical evaluations, we introduced a phenomenological linewidth with full-width-at-half-maximum(FWHM) of 4 meV for the A_{1s} , 30 meV for other A-exciton resonances and 40 meV for the B-series. The calculation agrees well with the experimentally observed peaks in energy as well as oscillator strengths, allowing for an unambiguous state assignment of the monolayer excitons.

Next, we apply the combined gap and DBE equations to compute the linear optical response for bilayer MoSe₂, using the same DFT parameters for the noninteracting band structure as for the monolayer. As long as one considers only the intralayer contributions, the Elliot formula[27] for an arbitrary layer within the multilayer structure is formally identical to that of a monolayer. However, quantitatively, the intralayer contributions are modified via their dependence on the detailed Coulomb matrix elements which are modified by both, the presence of the substrate and the other layers. As a result, each layer in a multilayer configuration experiences a different dielectric environment, generally leading to an intrinsic inhomogeneous broadening of the resonances due to the slightly different contributions from the individual layers. However, for an inversion symmetric bilayer, e.g. a suspended or encapsulated system, both layers are equivalent and resonances

corresponding to different intralayer excitons should be degenerate, and thus, do not give rise to *additional* resonances. For the encapsulated bilayer configuration at zero temperature and carrier density, we theoretically find the lowest *s*-type intra-layer resonances at $A_{1s} = 1624$ meV, $A_{2s} = 1759$ meV, and $A_{3s} = 1795$ meV, with a relative oscillator strength of 1, 1/5.71/16.3 respectively. Whereas the shift of the A_{2s} exciton resonance agrees with the experimental observations within an accuracy of 10%, the resonance positions and oscillator strengths of the $2s$ and $3s$ intralayer states do not match the experimental data, showing that these states are not responsible for the experimentally observed features.

In addition to the intralayer interactions, the theory predicts that the Coulomb attraction between electrons and holes in adjacent layers should give rise to additional bound interlayer excitons. For the encapsulated bilayer configuration, we find a binding energy of $E_{A_{1s}}^{\text{inter}} = 153$ meV for the interlayer exciton, only 27% less than the binding energy of $E_{A_{1s}}^{\text{intra}} = 209$ meV for the lowest intralayer exciton. As the interlayer exciton uses conduction-band states from the opposite K-valley, introducing a spin splitting of the conduction band leads to a blue shift of the A-interlayer exciton, and a simultaneous red shift of the B-intralayer exciton. Using a 20 meV spin splitting of the conduction band, we find the lowest interlayer exciton at $E_{1s}^{\text{inter}} = 1700$ meV, between the $1s$ and $2s$ resonances of the intralayer exciton. To determine the relative oscillator strength, we estimate the dipole matrix element for the inter-layer transition from the *d*-type Mo-orbital centered around the central *z* positions of the adjacent layers, giving $|p_{cv}^{n,n\pm 1}|^2/|p_{cv}^{n,n}|^2 \approx 0.2$. The resulting simulated spectrum for the encapsulated bilayer is shown in Fig. 2(c). The calculations have been performed assuming a 20 nm hBN capping, and we included a phenomenological broadening(FWHM) of 30 meV and 50 meV for A- and B- series, respectively. The results show excellent agreement with the experimentally observed spectra. With the quantitative agreement between theory and experiment, we assign the 1741 meV and 1711 meV peaks as A_{2s} exciton and A-interlayer exciton, respectively.

To further support our interpretation based on interlayer exciton states, we study the influence of thickness on the resonance position and oscillator strength in MoSe₂ multilayer systems. We prepare sample B (optical microscope image in Fig. 3(a), consisting of MoSe₂ monolayer, bilayer, trilayer, quad-layer and multilayers on a sapphire substrate. In Fig. 3(b), we show the measured reflection contrast for various sample thicknesses. The two main transitions around 1625 meV and 1875 meV correspond to the A_{1s} and B_{1s} excitons, respectively. Aside from these two features, we also observed the interlayer peak (1711 meV, blue dot) and A_{2s} shoulder (~ 1772 meV, green dot) in the bilayer spectrum. As the layer number increases, both intralayer exciton and interlayer exciton should show a redshift behavior due to increasing dielectric screening. Experimentally, the bulk intralayer species A_{1s} and B_{1s} redshift about 27 meV and 15 meV, respectively, from bilayer samples, whereas the observed A-interlayer shows a rather strong redshift of 47 meV as ap-

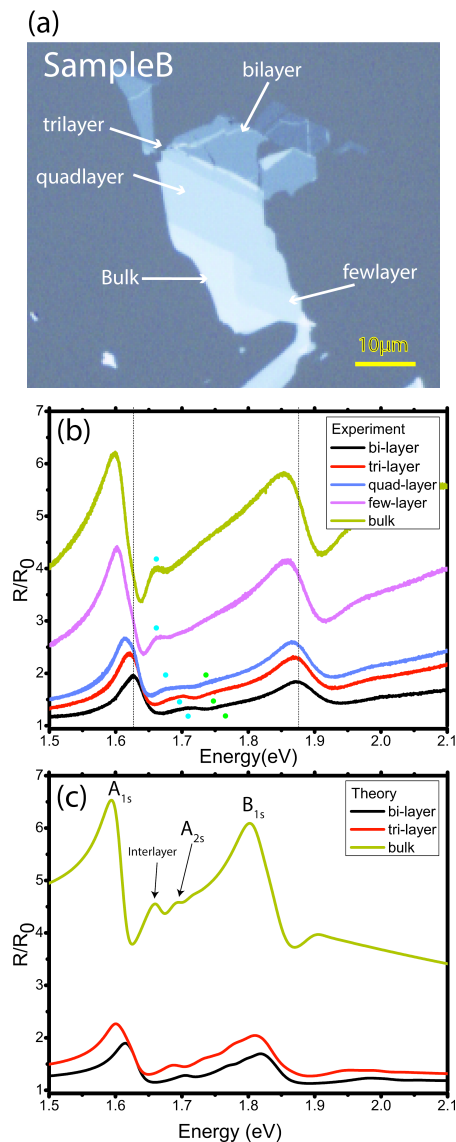


FIG. 3: (a) Optical microscope image of sample B, consisting of MoSe₂ layers with various thicknesses on a sapphire substrate. (b) Thickness dependence of experimental linear optical spectra. The interlayer exciton resonances are shown as red arrows and show red-shift and linewidth narrow as the sample approaching bulk limit. (c) Simulated optical spectra for the corresponding sample thickness.

proaching to the bulk limit. Similar to the monolayer, the shifts result from a simultaneously redshift of the interacting gap and exciton binding energy. As can be recognized, the interlayer exciton also becomes more apparent in the bulk limit. Apart from the narrower linewidth (35 meV in bilayer and 21 meV in bulk), which is expected due to reducing inhomogeneous broadening arising from the MoSe₂ surfaces, the reason for this is the relative oscillator strength. Whereas intralayer contributions increase linearly with the number of layers, the number of next neighbours and therewith the in-

terlayer contributions increase as $2(N - 1)$, thus doubling the relative oscillator strength $\Gamma^{\text{inter}}/\Gamma^{\text{intra}}$ going from bilayer to bulk.

We also perform DBE calculations to predict the linear optical response for numbers of layers. Again, we use the same monolayer DFT parameters including the same wavefunction overlap between adjacent layers. The computed optical spectra are plotted in Fig. 3(c). For the A-exciton series, we find good agreement with the experimental data in terms of both exciton resonance energies and oscillator strengths. In particular, we observe the increasing oscillator strength of the interlayer exciton compared to the intralayer exciton. Whereas the shifts of the B-excitons with increasing layer thickness is predicted very accurately, the theoretical results for the multilayers show a systematic red shift of the B-exciton series as compared with experiment, which is not apparent for the monolayer. This systematic discrepancy indicates that interlayer interactions might change the DFT bandstructure going from mono- to bilayer, which is not captured by our model system. Despite this shortcoming, the qualitative and quantitative agreement between theory and experiment provides strong evidence to assign the second peak to the interlayer exciton.

We note that in the ref. [28], the second-lowest feature in WS₂ reflection spectra was assigned to the A_{2s} exciton. According to our simulation and experiment, the correct assignment should be A-interlayer exciton.

At last, we compare the measured spectra of bilayer MoSe₂ with and without hBN encapsulation (Fig. 4(a)). The encapsulated sample is from sample A (bilayer in Fig. 2(a)) and the non-encapsulated sample is from sample B (bilayer in Fig. 3(a)). The computed spectra for the above sample structures are also plotted in Fig. 4(b) to show that our model well accounts for the excitonic shift in different screening environments. A direct observation is that both the intralayer and interlayer exciton peaks become sharper upon encapsulation. Recently, there are studies[29, 30] showing the hBN encapsulation provides a clean platform for high quality monolayer TMDC with narrow excitonic linewidth comparable with theoretical radiative broadening limit. We show that the encapsulation technique can also be applied to bilayer MoSe₂ for creating high quality samples. The intralayer exciton linewidth narrowing (from 46 meV to 20 meV for A_{1s} state) can be explained by reduced inhomogeneity with hBN interfaces as well as a more symmetric dielectric screening provided by hBN encapsulation, which removes the energy difference between intralayer excitons dwells in the top and bottom layer. The observed interlayer exciton also exhibits linewidth narrowing from 35 meV to 19 meV, enabling us to identify the interlayer peak unambiguously. Note that the interlayer exciton in current work shows a narrower linewidth and a much larger oscillator strength than those observed in TMD heterojunctions, which typically have linewidth around 50-100 meV and oscillator strength 1/100 of the A_{1s} state.[31–33]

In summary, the strongly confined quasi-particles in vdW layered semiconductors provide an interesting platform to

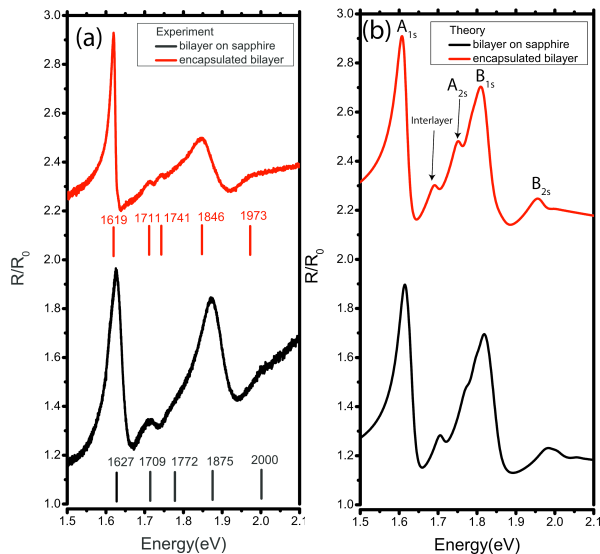


FIG. 4: (a) Comparison between optical spectra of MoSe₂ bilayer with hBN encapsulation (red curve) and without hBN encapsulation (black curve). The MoSe₂ bilayer with hBN shows a significant linewidth narrowing in both intralayer and interlayer excitonic transitions possibly due to symmetric dielectric screening and a clean environment. (b) Corresponding simulated optical spectra showing the theory is able to capture the dielectric screening effects on different exciton species.

form bound interlayer excitons. Through comparison between experimental and theoretical studies on linear optical spectra, we clearly identify the A-interlayer exciton in few-layer MoSe₂ systems. We first demonstrate that our DBE model reproduces the experimental monolayer MoSe₂ optical spectrum with a quantitative match and apply the same method to the few-layer MoSe₂ situation. The existence of interlayer excitons in layered single crystals substantiates the two-dimensional nature of electron behaviors, therefore our work is an essential step towards understanding the interlayer microscopic interactions in van der Waals materials.

The observed interlayer exciton has a large binding energy of 153 meV, suggesting high thermal stability compared with conventional spatially indirect excitons, and a linewidth of 19 meV, which is sharper than the interlayer exciton observed in TMD heterojunctions. Such strong Coulomb interaction in high quality vdWc materials suggest the possibility of using them as an interlayer exciton platform. Although the current interlayer exciton is in an indirect bandgap semiconductor, one can apply various methods to engineer the bandstructure of vdWc as well as the binding energy of excitons for creating long-lived interlayer excitons [15, 34, 35]. Our current work will provide a cornerstone for future fundamental research in interlayer excitons of 2D materials.

Acknowledgment The experimental work in Michigan is supported by the United States Army Research Office MURI

award W911NF-17-1-0312. The Marburg part of the work is a project of the Collaborative Research Center SFB 1083 funded by the Deutsche Forschungsgemeinschaft.

-
- [1] J. Frenkel, Physical Review **37**, 17 (1931).
 - [2] G. H. Wannier, Physical Review **52**, 191 (1937).
 - [3] M. Colocci, M. Gurioli, A. Vinattieri, F. Fermi, C. Deparis, J. Massies, and G. Neu, EPL (Europhysics Letters) **12**, 417 (1990).
 - [4] L. V. Butov, A. Zrenner, G. Abstreiter, G. Böhm, and G. Weimann, Phys. Rev. Lett. **73**, 304 (1994).
 - [5] A. K. Geim and I. V. Grigorieva, Nature **499**, 419 (2013).
 - [6] D. Jariwala, T. J. Marks, and M. C. Hersam, Nature Materials **16**, 170 (2016).
 - [7] P. Rivera, J. R. Schaibley, A. M. Jones, J. S. Ross, S. Wu, G. Aivazian, P. Klement, K. Seyler, G. Clark, N. J. Ghimire, J. Yan, D. G. Mandrus, W. Yao, and X. Xu, Nature Communications **6**, 6242 (2015).
 - [8] Philipp Nagler, Gerd Plechinger, Mariana V Ballottin, Anatolie Mitioglu, Sebastian Meier, Nicola Paradiso, Christoph Strunk, Alexey Chernikov, Peter C M Christianen, Christian Schller, and Tobias Korn, 2D Materials **4**, 025112 (2017).
 - [9] X. Zhu, N. R. Monahan, Z. Gong, H. Zhu, K. W. Williams, and C. A. Nelson, Journal of the American Chemical Society **137**, 8313 (2015).
 - [10] J. R. Schaibley, P. Rivera, H. Yu, K. L. Seyler, J. Yan, D. G. Mandrus, T. Taniguchi, K. Watanabe, W. Yao, and X. Xu, Nature Communications **7**, 13747 (2016).
 - [11] J. S. Ross, P. Rivera, J. Schaibley, E. Lee-Wong, H. Yu, T. Taniguchi, K. Watanabe, J. Yan, D. Mandrus, D. Cobden, W. Yao, and X. Xu, Nano Letters **17**, 638 (2017).
 - [12] L. Meckbach, T. Stroucken, and S. W. Koch, arXiv:1709.09056 (2017).
 - [13] L. Meckbach, T. Stroucken, and S. W. Koch, Submitted to Applied Physics Letters (2017).
 - [14] M. M. Fogler, L. V. Butov, and K. S. Novoselov, Nature Communications **5**, 4555 (2014).
 - [15] E. V. Calman, arXiv:1709.07043v1.
 - [16] Mathieu Alloing, Mussie Beian, Maciej Lewenstein, David Fuster, Yolanda Gonzalez, Luisa Gonzalez, Roland Combescot, Monique Combescot, and Francois Dubin, EPL (Europhysics Letters) **107**, 10012 (2014).
 - [17] Monique Combescot, Roland Combescot, and Francois Dubin, Reports on Progress in Physics **80**, 066501 (2017).
 - [18] J.-J. Su and A. H. MacDonald, Phys. Rev. B **95**, 045416 (2017).
 - [19] O. L. Berman and R. Y. Kezerashvili, Phys. Rev. B **96**, 094502 (2017).
 - [20] H. Deng, H. Haug, and Y. Yamamoto, Reviews of Modern Physics **82**, 1489 (2010).
 - [21] I. Carusotto and C. Ciuti, Reviews of Modern Physics **85**, 299 (2013).
 - [22] M. Ye, D. Winslow, D. Zhang, R. Pandey, and Y. K. Yap, Photonics **2**, 288 (2015).
 - [23] X. Xu, W. Yao, D. Xiao, and T. F. Heinz, Nature Physics **10**, 343 (2014).
 - [24] D. Xiao, G.-B. Liu, W. Feng, X. Xu, and W. Yao, Phys. Rev. Lett. **108**, 196802 (2012).
 - [25] In the massive Dirac-Fermion for MoSe₂ layers, we use the parameters the energy gap $\Delta = 1.47$ eV, the effective hopping matrix element $t = 0.94$ eV, the lattice constant $a = 3.313$ Å and

the spin splitting of valence and conduction band $2\lambda_v = 0.18$ eV and $2\lambda_c = 0.02$ eV, as given in Ref.[24?]. The in-plane and out-of-plane background dielectric constants are 3.36 and 5.16, respectively. Furthermore, we use a natural layer-to-layer distance of $D = 6.5 \text{ \AA}$ and an effective thickness parameter characterizing the finite extension of the Mo- d -orbitals in out-of-plane direction of 5 \AA .

- [26] J. M. Riley, F. Mazzola, M. Dendzik, M. Michiardi, T. Takayama, L. Bawden, C. Graner, M. Leandersson, T. Balasubramanian, M. Hoesch, T. K. Kim, H. Takagi, W. Meevasana, P. Hofmann, M. S. Bahramy, J. W. Wells, and P. D. C. King, *Nature Physics* **10**, 835 (2014).
- [27] H. Haug and S. W. Koch, *Quantum Theory of the Optical and Electronic Properties of Semiconductors*, 5th ed. (World Scientific Publishing, Singapur, 2009).
- [28] A. Chernikov, T. C. Berkelbach, H. M. Hill, A. Rigosi, Y. Li, and O. B. Aslan, *Phys. Rev. Lett.* **113**, 076802 (2014).
- [29] F. Cadiz, E. Courtade, C. Robert, G. Wang, Y. Shen, H. Cai, T. Taniguchi, K. Watanabe, H. Carrere, D. Lagarde, M. Manca, T. Amand, P. Renucci, S. Tongay, X. Marie, and B. Urbaszek, *Phys. Rev. X* **7**, 021026 (2017).
- [30] O. A. Ajayi, J. V. Ardelean, G. D. Shepard, J. Wang, A. Antony, T. Taniguchi, K. Watanabe, T. F. Heinz, S. Strauf, X.-Y. Zhu, and J. C. Hone, *2D Materials* **4**, 031011 (2017).
- [31] Michael Frg, Lo Colombier, Robin K. Patel, Jessica Lindlau, Aditya D. Mohite, Hisato Yamaguchi, David Hunger, and Alexander Hgele, arXiv:1710.00990v2.
- [32] B. Miller, A. Steinhoff, B. Pano, J. Klein, F. Jahnke, A. Holleitner, and U. Wurstbauer, *Nano Letters* **17**, 5229 (2017).
- [33] M. Baranowski, A. Surrente, L. Klopotoski, J. M. Urban, N. Zhang, D. K. Maude, K. Wiwatowski, S. Mackowski, Y. C. Kung, D. Dumcenco, A. Kis, and P. Plochocka, *Nano Letters* **17**, 6360 (2017).
- [34] Y.-H. Zhao, F. Yang, J. Wang, H. Guo, and W. Ji, *Scientific Reports* **5**, 8356 (2015).
- [35] D. Lloyd, X. Liu, J. W. Christopher, L. Cantley, A. Wadehra, B. L. Kim, B. B. Goldberg, A. K. Swan, and J. S. Bunch, *Nano Letters* **16**, 5836 (2016), pMID: 27509768.